Temperature dependence of homogeneous broadening of the 1*S* paraexciton in Cu_2O

Jan Brandt,* Patrick Felbier, Dietmar Fröhlich, Christian Sandfort, and Manfred Bayer
Institut für Physik, Technische Universität Dortmund, D-44221 Dortmund, Germany

Heinrich Stolz
Fachbereich Physik, Universität Rostock, D-18051 Rostock, Germany

(Received 17 November 2009; revised manuscript received 19 February 2010; published 28 April 2010)

We report on polariton propagation beats of the yellow 1*S* paraexciton in Cu_2O as function of magnetic field, laser energy, and temperature. The propagation beats are fitted by a model including the inhomogeneity of the sample, which enables us to distinguish between homogeneous damping and inhomogeneous broadening. By use of a ^{3}He insert we achieved bath temperatures down to 0.35 K. Propagation beats of a 13 ns Gaussian laser pulse were observable up to 180 ns after the pulse leading to a remarkably small homogeneous damping of about 9 neV at the lowest temperature. The corresponding dephasing time is 150 ns decreasing rapidly to about 5 ns at 2.1 K. These results are confirmed by absorption spectra of the same sample. The temperature dependence of the homogeneous damping is discussed in terms of longitudinal-acoustic phonon scattering.

DOI: 10.1103/PhysRevB.81.155214 PACS number(s): 78.20.−e, 71.35.Cc, 71.36.+c

I. INTRODUCTION

Since the first observation of Bose-Einstein condensation (BEC) in an atomic gas,[1,2] many attempts to observe the phenomenon of spontaneous coherence in solid-state systems have been made.[3] For a long-time promising candidates have been the 1*S* excitons of the yellow series in Cu_2O, which consist of the paraexciton (irreducible representation Γ_2^+) and the three quadrupole allowed orthoexcitons (Γ_5^+), which are split off by ϵ=12.12 meV (Ref. 4) due to isotropic short-range exchange. The paraexciton is a pure spin-triplet state and therefore it is optically forbidden to all orders of electric transitions because of symmetry and spin selection rules. In a magnetic field, however, it becomes optically allowed and shows an extremely narrow resonance. The paraexciton mass was determined to $M_P=2.61m_0$ (Ref. 5) allowing one to evaluate the critical density for a BEC transition.

Due to its long lifetime of about 1 μs (Refs. 6 and 7) a resonantly excited paraexciton gas can thermalize with the phonon bath.[8] At densities close to the critical density at 2 K, however, the lifetime is strongly reduced by the bimolecular decay,[9] which results in a decay time of about a nanosecond and prevents crossing the phase boundary. Additionally, the exciton gas is heated and thermalization is affected by exciton-exciton interaction. The reported thermalization time of a few hundred nanoseconds[7] and the expected phonon-scattering time of a few nanoseconds,[10] however, are inconsistent.

Up to now, all attempts to optically excite a critical density either resonantly or nonresonantly have failed and all claims for a BEC of 1*S* excitons in Cu_2O have been rejected.[3] There were only a few experiments in which exciton densities were determined quantitatively.[11,12] As the bimolecular decay seems to prevent reaching the critical density in a ^{4}He bath, further cooling in a ^{3}He bath or in a ^{3}He/^{4}He dilution refrigerator might help to reach the critical density. For an exciton BEC in thermal quasiequilibrium with the phonon bath at very low temperatures, however, a sufficiently high acoustic phonon-scattering rate is essential.

In high-purity samples at low temperatures, the acoustic phonon-scattering rate determines the polariton damping for low particle densities. This damping can be determined by energy- or time-resolved transmission experiments, either from the linewidth of the absorption spectrum or from the decay of polariton propagation beats. Four-wave mixing, the common method for the determination of dephasing, is not practical for long dephasing times in the range of tens or hundreds of nanosecond as they are expected for the paraexciton due to its long lifetime and small phonon coupling. The appearance of propagation beats is already well known for the 1*S* orthoexcitons in Cu_2O (Ref. 13) and first measurements of paraexciton beats at 1.2 K were reported recently.[14]

In this contribution we present paraexciton polariton propagation beats and compare the results to transmission spectra for varying magnetic field, laser energy, and temperature. The temperature dependence of the polariton damping and dephasing time is determined from fits of the propagation beats. We observe paraexciton polariton dephasing times up to 150 ns at 0.35 K, which drastically drop to about 5 ns at 2.1 K.

In Sec. II, we present the theory of paraexciton polaritons, which is used to fit the propagation beats and calculate the paraexciton longitudinal-acoustic (LA)-phonon-scattering rate. The experimental setup is described in Sec. III. Our results are discussed in Sec. IV, followed by conclusions (Sec. V) and the Appendix with a derivation of the relevant equations.

II. THEORY

Due to symmetry and spin selection rules the paraexciton is optically forbidden to all orders. In a magnetic field the paraexciton mixes with the orthoexcitons, in strain fields additionally with excitons of the green series, and thus becomes weakly allowed.[6,15] For a magnetic field the coupling to the orthoexcitons can be described in the basis of the paraexciton P and the three orthoexcitons $M=0,\pm1$ by the matrix

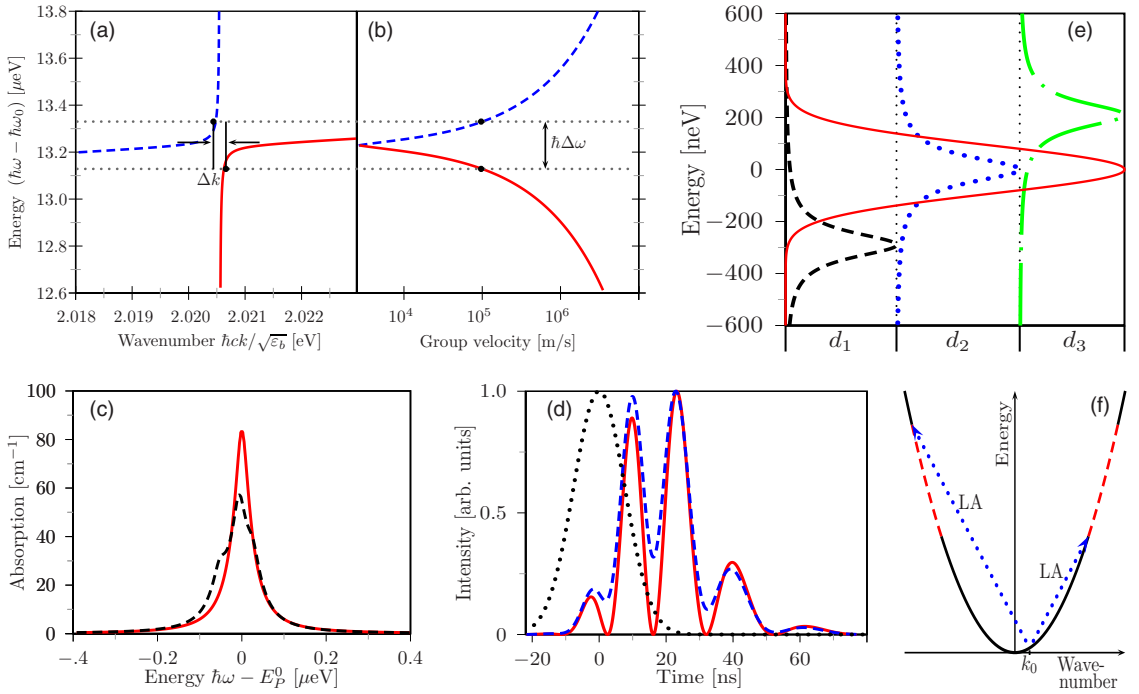

FIG. 1. (Color online) (a) Undamped paraexciton polariton dispersion $\hbar\omega(k)$ close to the polariton resonance at 13.2 μeV for a magnetic field $B=7$ T; $\hbar\omega_0$ is the paraexciton band minimum at $k=0$; red solid line, lower polariton branch; blue dashed line, upper polariton branch; and the dotted horizontal lines mark polaritons with a group velocity $v_g=10^5$ m/s, whose wave vectors differ by Δk. (b) Group velocity v_g for the dispersion in (a); blue dashed line, v_g for the upper branch; red solid line, v_g for the lower branch; the dotted horizontal lines mark the two states with $v_g=10^5$ m/s, both polariton states differ by Δk in their wave vector and $\hbar\Delta\omega$ in their energy. (c) Calculated absorption of the paraexciton resonance in a magnetic field of 7 T for a sample of thickness $d=5.5$ mm with a damping $\Gamma=60$ neV, $E_P^0=2.02064$ eV is the paraexciton resonance at $B=7$ T; red solid line, absorption of a homogeneous sample; and black dashed line, absorption of an inhomogeneous sample as sketched in (e). (d) Normalized transmitted intensity of an incoming Gaussian pulse as function of time [see Eq. (3)]; black dotted line, Gaussian pulse with FWHM=13 ns; red solid line, time-resolved transmission of the Gaussian pulse in the paraexciton resonance through a sample of thickness $d=5.5$ mm with the damping as in (c); blue dashed line, transmission of a pulse detuned by 30 neV from the paraexciton resonance. (e) Sketch of a sample consisting of three layers with different resonances shown as a black dashed, blue dotted, and green dashed-dotted Lorentzian, the amplitudes of the Lorentzians correspond to the thicknesses d_j of the layers; red solid line, laser spectrum (Gaussian with FWHM=150 μeV). (f) Schematics of the intraband LA-phonon scattering, k_0 marks the resonance wave number; exciton parabola, black solid line; LA phonons, blue dotted arrows; and region of final states, red dashed part of parabola.

$$H_B = \begin{pmatrix} -\varepsilon & i\alpha B & 0 & 0 \\ -i\alpha B & 0 & 0 & 0 \\ 0 & 0 & \beta B & 0 \\ 0 & 0 & 0 & -\beta B \end{pmatrix} \tag{1}$$

with the coefficients $\alpha=92.5$ μeV/T and $\beta=47.7$ μeV/T.[15] As the paraexciton becomes quadrupole allowed it has to be treated as a polariton with the dispersion

$$\frac{c^2k^2}{\omega^2} = \varepsilon_b + \frac{f_P\hbar^2c^2k^2}{\left(\hbar\omega_0 + \dfrac{\hbar^2k^2}{2M_P}\right)^2 - (\hbar\omega)^2 - i\Gamma\hbar\omega}, \tag{2}$$

where the background dielectric constant $\varepsilon_b=8.61$,[5] the mass $M_P=2.61m_0$, the oscillator strength $f_P=5.6\times10^{-5}f_O\cdot B^2$, and the paraexciton band minimum $\hbar\omega_0(B)=2.02066$ eV $-(\alpha\cdot B)^2/\epsilon$.[14,15] The phenomenological damping Γ in Eq. (2) takes into account recombination and scattering of the propagating polaritons with phonons and impurities, and describes dephasing and absorption.

The dispersion [Eq. (2)] without damping ($\Gamma=0$) yields for $\omega\geq\omega_0$ two solutions $\omega(k)$. In Fig. 1(a) these two branches are shown for energies close to the resonance. For a finite damping the situation changes and at each energy two complex solutions exist. The electric field linked to these two modes propagating through a sample of thickness d is given by

$$E(d,\omega) = \sum_{j=1}^{2} a_j(k_j,\omega)\exp(ik_jd), \tag{3}$$

where the complex coefficients

$$a_j(k_j,\omega) = \frac{k_{i\neq j}^2(\omega) - \varepsilon_b(\omega/c)^2}{k_{i\neq j}^2(\omega) - k_j^2(\omega)}, \quad (i,j) \in \{(1,2),(2,1)\}$$

are derived from Maxwell's boundary conditions and Pekar's additional boundary conditions (ABC) at the sample

surface.[16] Each polariton branch contributes with a different absorption coefficient and due to Eq. (3) both interfere with each other. Hence, the absorption spectrum of a sample of thickness d is calculated from Eq. (3) as $\alpha(\omega)\cdot d = -\log(|E(d,\omega)|^2/|E(0,\omega)|^2)$ [see Fig. 1(c)].

The time-resolved transmission of the field of a laser pulse E_L is calculated by the Fourier transform of $E(d,\omega)$ [Eq. (3)] and the spectrum of the pulse $E_L(\omega)$,

$$E(d,t) \propto \sum_{j=1}^{2} \int_{-\infty}^{\infty} a_j(k,\omega) E_L(\omega) \exp(i[k_j d - \omega t]) d\omega. \quad (4)$$

As shown in Figs. 1(a) and 1(b), there are polariton states with equal group velocity $v_g = d\omega/dk$ on both branches; the crossing of the two dashed horizontal lines with the upper and lower branches mark polaritons with equal group velocity of $v_g = 10^5$ m/s. Though both polaritons reach the back surface of the sample at the same time, they obtain a phase shift $\Delta\Phi$ due to their difference in k and ω [see Figs. 1(a) and 1(b)]. The total phase shift is $\Delta\Phi(d) = (\Delta k - \Delta\omega/v_g)d$. As the phase shift depends on ω, and thus on the group velocity v_g, it changes with time leading to beats in the time-resolved transmission. The period of these beats decreases with increasing thickness d, and also with increasing external magnetic field B, since the oscillator strength f_P increases with B^2 [Eq. (2)]. The damping Γ describes the decay of the amplitude of the beats. Propagation beats are observable as long as $\Gamma/\gamma_l \ll 1$ holds,[17] where Γ is the polariton damping and $\gamma_L = h/\tau_L$ is the spectral width of the laser pulse. Figure 1(d) shows calculated beats (solid line) for a resonant laser pulse, propagating through a crystal of thickness $d = 5.5$ mm at $B = 7$ T for a damping $\Gamma = 60$ neV. Also shown in Fig. 1(d) are propagation beats for a laser pulse detuned from resonance (dashed line). The most significant changes are the nonzero minima of the beats in the latter case. As an example for the effect of inhomogeneity we consider a sample of three layers with slightly different resonances [Fig. 1(e)]. Since the laser is not on resonance in each layer, beats similar to the off-resonance case shown in Fig. 1(d) (dashed line) are expected. For such a sample the transmission can be calculated using Maxwell boundary conditions between the different layers. The spectrum is basically the product of the transmission spectra of the three layers, in certain cases distinct absorption features could be observed as plotted by the dashed line in Fig. 1(c) for the case of the sketched inhomogeneous sample [see Fig. 1(e)]. The equations for the calculation of the transmitted field are derived in the Appendix. Again the time-resolved transmission can be calculated by the Fourier transform of the convolution of an incoming pulse and the transmission of the field $E(d,\omega)$ [see Eq. (3)].

The phenomenological damping Γ in Eq. (3) describes the dephasing due to recombination, scattering by phonons and impurities. Since the exciton lifetime $T_1 \approx 1$ μs (Refs. 6 and 7) is quite long for a bulk semiconductor, it is expected to be insignificant as a dephasing mechanism. For symmetry reasons the paraexciton couples only to LA phonons and not to transverse-acoustic phonons.[18] Thus, at low temperatures in high quality samples with a low impurity density scattering with LA phonons is expected to be the main dephasing mechanism. As shown in Fig. 1(f), we need only to take into account anti-Stokes scattering out of the resonance state k_0 due to energy and momentum conservation. In order to calculate the anti-Stokes scattering rate $\Gamma_{AS}(E,T)$ for an occupation $N_{E_P^0}$ of paraexcitons at the resonance energy E_P^0 we use the equations given in Ref. 10 neglecting stimulated scattering events since we have low exciton densities and low temperatures. As $\Gamma_{AS}(E,T)$ is almost independent of E around the resonance E_P^0, we neglect its energy dependence and set $\Gamma(T) = \Gamma_{AS}(E_P^0,T)$. With the energy $\tilde{E} = E/e_0$ and temperature $\tilde{T} = k_B \cdot T/e_0$ scaled to $e_0 = 2 \cdot M_P \cdot v_{\mathrm{LA}}^2$ this yields

$$\frac{\partial N_{\tilde{E}_P^0}}{\partial \tau} = -\Gamma(\tilde{T}) \cdot N_{\tilde{E}_P^0},$$

$$\Gamma(\tilde{T}) = \frac{1}{\tau_{sc}} \frac{1}{2 \cdot \sqrt{\tilde{E}_P^0}} \int_{(\sqrt{\tilde{E}_P^0}-1)^2}^{(\sqrt{\tilde{E}_P^0}+1)^2} (\tilde{E}_P^0 - \tilde{E}_1)^2 \cdot \frac{1}{\exp[(\tilde{E}_P^0 - \tilde{E}_1)/\tilde{T}] - 1} \cdot d\tilde{E}_1, \quad (5)$$

where the characteristic scattering time scale is given by

$$\tau_{sc} = \frac{\pi \hbar^4 \rho}{2 D_{\mathrm{LA}}^2 \cdot M_P^3 \cdot v_{\mathrm{LA}}}$$

with the deformation potential $D_{\mathrm{LA}} = 1680$ meV,[19] the LA sound velocity $v_{\mathrm{LA}} = 4.63 \cdot 10^3$ m/s,[5] and the mass density $\rho = 6.1$ g/cm^3.[20] From the damping Γ one can estimate the dephasing time $T_2 = 2\hbar/\Gamma$ of the paraexcitons. The derivation of Eq. (5) is explained in greater detail in the Appendix.

III. EXPERIMENTAL SETUP

A single frequency dye laser (linewidth 5 neV) is modulated by an electro-optical modulator to generate Gaussian pulses with a full width at half maximum (FWHM) of 13 ns. The repetition rate of 160 kHz ensures a dark time much longer then the paraexciton lifetime. For a maximum continuous-wave laser power of 50 mW, we thus get an average power of only 110 μW. Taking into account reflection losses we expect 63 μW in the sample. For the measurements at very low temperatures (^{3}He cryostat) we lower the average power in the crystal to about 20 μW.

For measurements between 1.2 and 2.2 K, a ^{4}He split coil cryostat (magnetic field up to 10 T) and between 0.3 and 1.3 K a ^{3}He split coil cryostat (7 T) is used. The ^{3}He insert is a closed cycle system consisting of a ^{3}He gas storage, a 1 K pot cooled by superfluid ^{4}He to condense the gas, and a sorption pump for further cooling of the condensed ^{3}He. The sample is immersed in the ^{3}He bath.

The transmitted pulse is detected by a fast photo diode (bandwidth 1.4 GHz) and a digital oscilloscope (bandwidth 1.5 GHz), the overall time resolution is about 1 ns. A diaphragm is used as a spatial filter to suppress scattered light on the diodes. In order to clearly resolve the beats, long

delay times up to 100 ns are necessary, which are achieved with samples of several millimeter thickness. The sample of $d=5.5$ mm thickness is cut from a high quality natural crystal, oriented by x-ray diffraction, and mounted strain free in the cryostat. The sample was mounted with $\mathbf{k}\|[11\bar{2}]$ and $\mathbf{B}\|[1\bar{1}0]$.

We got clear beats only in one sample but for two different k directions ($[11\bar{2}]$ and $[111]$). Because of the higher oscillator strength (factor of 2) we have done the measurements in the $[11\bar{2}]$ direction. Other crystals of less homogeneity showed only indications of beats. Further details about the setup can be found elsewhere.[21]

IV. RESULTS AND DISCUSSION

In Fig. 2 paraexciton propagation beats for different magnetic fields are shown. Clearly the beat period increases with increasing delay times. With increasing magnetic field, and thus increasing oscillator strength, the period decreases. Due to inhomogeneous broadening, the beat minima are nonzero. Since the field dependence of the oscillator strength is well known,[4] we can determine the inhomogeneous broadening. For example, fits without and with inhomogeneous broadening are compared in Fig. 2 for a magnetic field of 6 T. Both curves differ in the beat period and the minima. Obviously, taking into account inhomogeneous broadening gives a better fit of the data.

Propagation beats for different detuning from resonance are plotted in Fig. 3. As also demonstrated by the calculated curve in the inset of Fig. 1(d), the beats have finite minima, whose values increase with increasing detuning from resonance. Additionally, the number and the time range of observable beat maxima decreases due to the increasing group velocity outside the resonance. Since the paraexciton is inhomogeneously broadened, the minima are also nonzero in resonance. Paraexciton beats, as measured with the laser in resonance, are observable up to 60 ns. This is clear evidence for a long dephasing time and a small polariton damping Γ.

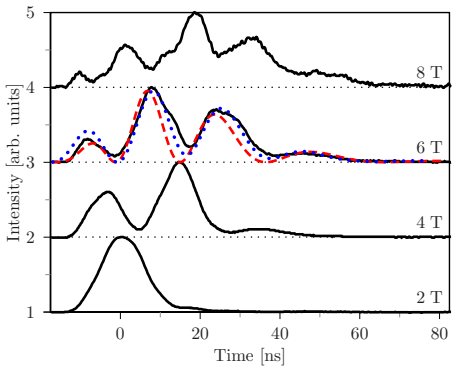

FIG. 2. (Color online) Propagation beats for different magnetic fields from 2 to 8 T, the magnetic field for each curve is noted on the right, laser was in resonance at each field, $T=1.2$ K; black lines, experimental data; red dashed line, calculation for $B=6$ T without inhomogeneous broadening; and blue dotted line, fit with inhomogeneous broadening.

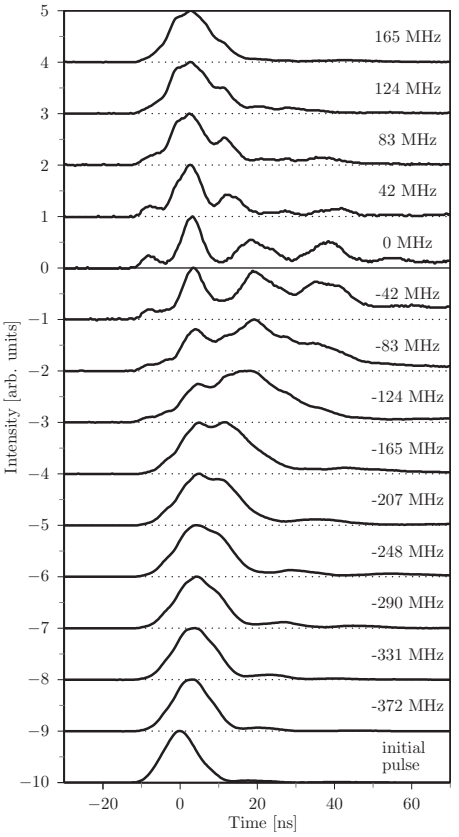

FIG. 3. Paraexciton propagation beats as function of laser detuning from resonance. Beats were measured in a magnetic field $B=7$ T at a bath temperature of 0.4 K. The laser detuning of each curve is shown on the right.

In Fig. 4 propagation beats for different bath temperatures are shown. We used two different cryostats (with ^{3}He or ^{4}He as coolant) and the same focusing lens for both cryostats. We thus expect to have the same focus diameter ($d\propto 30$ μm). By checking the transmission spectrum prior to our beat measurements we were able to select similar spots on the sample which turned out to be very homogeneous across the surface of about 5×5 mm^2. Obviously, the number of oscillations decreases with increasing temperature. This accelerated decay of the amplitude reflects the decrease in the dephasing time, which corresponds to an increase in the polariton damping. The beat curves are fitted by the model described in Sec. II using three layers with different resonances (parameters see Fig. 4). A three-layer model for the inhomogeneity is used since tests with up to seven layers yield the same results for the inhomogeneous broadening and homogeneous damping.

The analysis directly yields the damping as function of bath temperature. We observed beats for more than 180 ns at 0.35 K reflecting a very small paraexciton polariton damping, the fit yielded a minimum damping $\Gamma=9$ neV corresponding to a dephasing time $T_2=150$ ns. The results of the fits are compared with the resonance transmission spectra as shown in Fig. 5, where the measured spectra and the sum of three Lorentzians with the parameters from the fit of the beats are plotted for different temperatures. In the range of

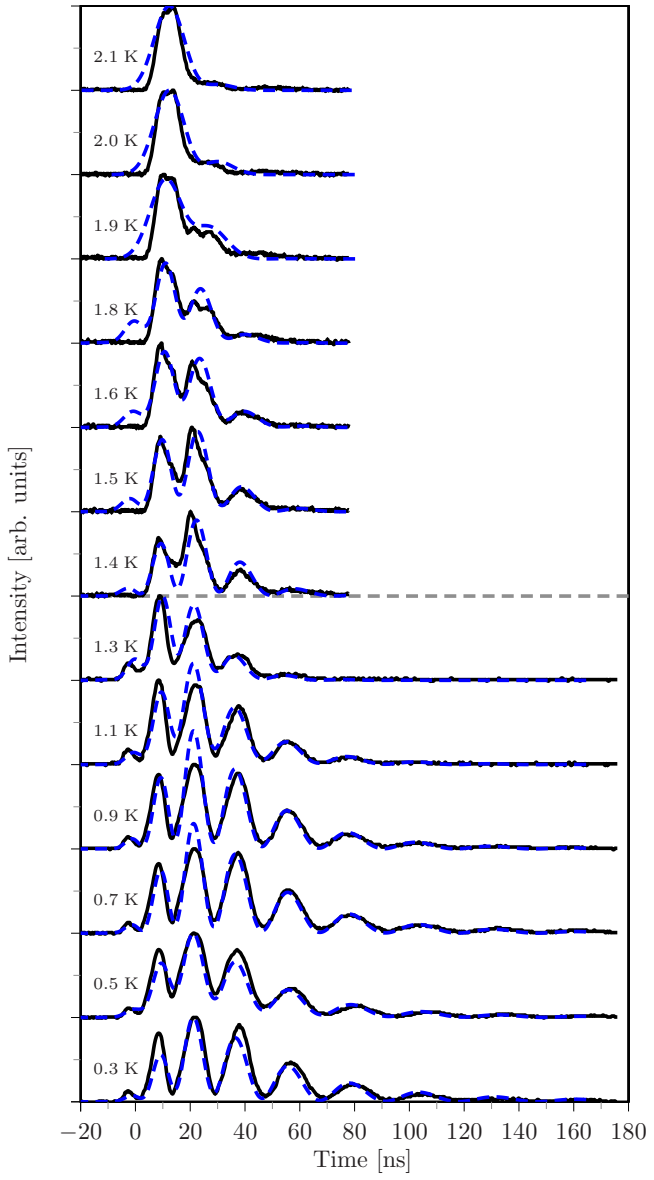

FIG. 4. (Color online) Propagation beats in a magnetic field of 7 T for different temperatures. Temperatures up to 1.3 K in liquid ^{3}He bath, higher temperatures (curves above dashed line) in superfluid ^{4}He. Black lines, measured data and blue dashed lines, fits as described in the text. Inhomogeneity parameters: for ^{3}He data layer thicknesses 1.7, 1.8, and 2.0 mm and resonance detuning −38, −2, and 37 neV are used, for the ^{4}He data 2.2, 2.2, and 1.1 mm and −39, −20, and 0 neV.

the pulse spectrum (blue dotted line) the calculated and the measured spectra agree well.

The polariton damping Γ as function of temperature is shown in Fig. 6 (full dots). The damping increases from 9 up to 170 neV in a temperature range of less than 2 K. Additionally, the LA-phonon-scattering rate as discussed in the previous section is plotted as the black solid line. At lowest temperatures the measured polariton damping and the calculated phonon-scattering rate differ. There are two possible reasons for this deviation. First, the cooling efficiency of liquid ^{3}He is reduced at lowest temperatures due to the Kapitza resistance[22] and the exciting laser light heats the

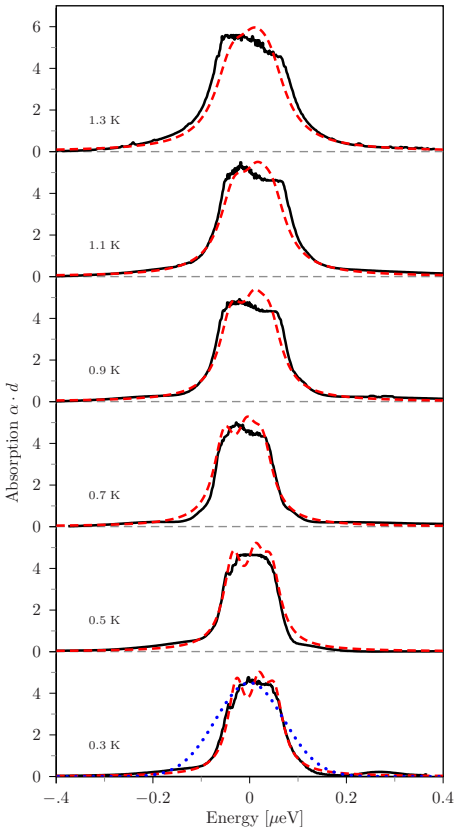

FIG. 5. (Color online) Paraexciton absorption spectrum as function of temperature for the same configuration as in Fig. 4 (B =7 T), measured with continuous-wave laser (spectral width 5 neV); black lines, measured spectra; red dashed lines, sum of three Lorentzians with parameters from the fit of the corresponding beats; blue dotted line, spectrum of the Gaussian laser pulse.

sample, which results in an increased homogeneous damping. For the ^{3}He experiments we used very low average laser power (about 20 μW). Heating of the sample should thus not be the cause for the deviations of the damping from the phonon-scattering rate. Second, despite the high quality of

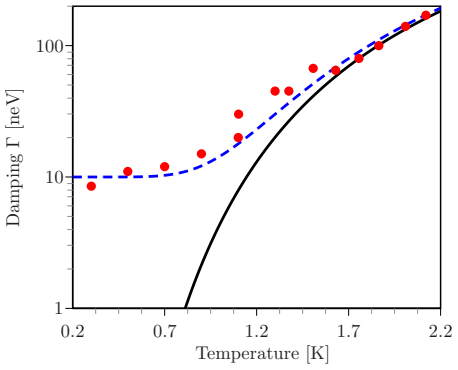

FIG. 6. (Color online) Homogeneous damping Γ of the paraexciton polariton as function of the bath temperature at B=7 T (red dots), plotted on a logarithmic scale. The black solid line shows the calculated LA-phonon-scattering rate, the blue dashed line is the sum of the LA-phonon-scattering rate and an impurity damping of 10 neV.

our sample it contains still some impurities and, since at lowest temperatures the phonon-scattering rate vanishes, the scattering of the polaritons by impurities becomes important. From the data we determine an impurity polariton damping of about 10 neV in this sample. As thermal equilibrium is reached within a few phonon-scattering events, thermalization time at 2 K is a few tens of nanosecond in contrast to the results by Fishman *et al.*[7] Because of the high energy pumping their experimental conditions cannot be compared to our resonant pumping experiment.

In the propagation beats experiments high-density effects are not studied due to the limited number of polaritons generated in one duty cycle. At 0.4 K we observed a decreasing number of oscillations with increasing power. This was probably due to heating because the ^{3}He cooling efficiency is limited by the Kapitza resistance. Nevertheless it would be an interesting project to study the density dependence at the lowest temperature with ^{4}He cooling (1.2 K). Because of the limited laser power (about 50 mW) we are not able to excite within the 13 ns pulse enough polaritons to reach high enough densities. With use of a power laser it should be feasible to study high-density effects by beat spectroscopy. One would then expect dramatic effects due to the bimolecular decay.[9]

V. CONCLUSIONS

Paraexciton polariton propagation beats show a decreasing period with increasing magnetic field, the shape changes drastically as the laser is detuned from resonance. With increasing temperature the number of oscillations decreases due to an increased phonon-scattering rate. The shape of the measured propagation beats can be reproduced by taking into account the inhomogeneity of the sample, which allows us to determine the polariton damping and dephasing time. We observe dephasing times up to 150 ns at 0.35 K and 5 ns at 2.1 K. The dephasing at the lowest temperature is most likely caused by polariton-impurity scattering. Due to the decreased phonon-scattering rate, the thermalization of the excited polaritons with the bath becomes less effective for low temperatures. Even though the thermalization time remains almost unchanged below 1 K, a ^{3}He bath does not improve the chances for a paraexciton condensate, since at low temperatures thermalization of the exciton gas with the phonon bath becomes inefficient, and high excitation densities heat the exciton gas and the sample. A dilution refrigerator might be more effective for this purpose. Anyhow, a paraexciton BEC will not be in thermal equilibrium with the phonon bath since at low temperatures the LA scattering rate becomes much smaller than the high-density exciton lifetime.

ACKNOWLEDGMENTS

We acknowledge the support by the Deutsche Forschungsgemeinschaft (SFB "Starke Korrelationen im Strahlungsfeld" and Forschergruppe "Quantenoptik in Halbleitern").

APPENDIX

1. LA-scattering rate

The LA-phonon-scattering rate [Eq. (5)] is derived starting from Eq. (2) in Ref. 10,

$$\frac{\partial}{\partial t}N_E = -\frac{\sqrt{M_P}D_{\mathrm{LA}}^2}{4\sqrt{2}\pi\hbar^4 v_{\mathrm{LA}}^4 \rho\sqrt{E}}\int dE_1 (E-E_1)^2 \{[N_E(1+n^{ph}_{E-E_1})(1+N_{E_1}) - (1+N_E)n^{ph}_{E-E_1}N_{E_1}]$$
$$\cdot \Theta(q_S - \sqrt{E}+\sqrt{E_1})\cdot\Theta(-q_S+\sqrt{E}+\sqrt{E_1})\cdot\Theta(E-E_1)$$
$$+[N_E n^{ph}_{E_1-E}(1+N_{E_1}) - (1+N_E)(1+n^{ph}_{E_1-E})N_{E_1}]\cdot\Theta(q_{AS}-\sqrt{E_1}+\sqrt{E})\cdot\Theta(-q_{AS}+\sqrt{E_1}+\sqrt{E})\cdot\Theta(E_1-E)\}, \quad \text{(A1)}$$

where $n_E^{ph} = \frac{1}{\exp(-E/(k_B T))-1}$ and $q_{S|AS} = \pm(E-E_1)/(\sqrt{2M_P}v_{\mathrm{LA}})$. For low excitation intensities the occupation of excitons is low and stimulated scattering events can be neglected. With the characteristic scattering time

$$\tau_{sc} = \frac{\pi\hbar^4\rho}{2D_{\mathrm{LA}}^2 \cdot M_P^3 \cdot v_{\mathrm{LA}}}$$

one obtains

$$\frac{\partial}{\partial t}N_E = -\frac{1}{8M_P^{5/2}v_{\mathrm{LA}}^5\tau_{sc}\sqrt{2}\sqrt{E}}\int dE_1 (E-E_1)^2\{[N_E(1+n^{ph}_{E-E_1}) - n_{E-E_1}N_{E_1}]\cdot\Theta(q_S-\sqrt{E}+\sqrt{E_1})\cdot\Theta(-q_S+\sqrt{E}+\sqrt{E_1})\cdot\Theta(E-E_1)$$
$$+[N_E n^{ph}_{E_1-E} - (1+n^{ph}_{E_1-E})N_{E_1}]\cdot\Theta(q_{AS}-\sqrt{E_1}+\sqrt{E})\cdot\Theta(-q_{AS}+\sqrt{E_1}+\sqrt{E})\cdot\Theta(E_1-E)\}. \quad \text{(A2)}$$

Due to energy and momentum conservation [see Fig. 1(f)], for excitons at the quadrupole resonance E_P^0 only anti-Stokes scattering is possible, which yields

$$\frac{\partial}{\partial t}N_{E_P^0} = -\frac{1}{8M_P^{\frac{5}{2}}v_{\mathrm{LA}}^5\tau_{sc}\sqrt{2}\sqrt{E_P^0}}\int dE_1(E_P^0 - E_1)^2[N_{E_P^0}n_{E_1-E_P^0}^{ph} - (1+n_{E_1-E_P^0}^{ph})N_{E_1}]\cdot\Theta(q_{AS}-\sqrt{E_1}+\sqrt{E_P^0}) \cdot\Theta(-q_{AS}+\sqrt{E_1}+\sqrt{E_P^0})\cdot\Theta(E_1-E_P^0). \tag{A3}$$

Since in the experiment only excitons at the resonance E_P^0 are created, scattering events from an energy E_1 to the resonance E_P^0 are rather unlikely due to the low occupation N_{E_1} and do not have much impact on the damping. One thus obtains

$$\frac{\partial}{\partial t}N_{E_P^0} = -\frac{1}{8M_P^{5/2}v_{\mathrm{LA}}^5\tau_{sc}\sqrt{2}\sqrt{E_P^0}}\int dE_1\cdot(E_P^0 - E_1)^2 \cdot N_{E_P^0}n_{E_1-E_P^0}^{ph}\cdot\Theta(q_{AS}-\sqrt{E_1}+\sqrt{E_P^0}) \cdot\Theta(-q_{AS}+\sqrt{E_1}+\sqrt{E_P^0})\cdot\Theta(E_1-E_P^0). \tag{A4}$$

Scaling the energy and temperature in multiples of $e_0 = 2\cdot M_P\cdot v_{\mathrm{LA}}^2$, and introducing $\tilde{E}=E/e_0$ and $\tilde{T}=k_B\cdot T/e_0$, leads to

$$\frac{\partial}{\partial t}N_{\tilde{E}_P^0} = -\frac{1}{\tau_{sc}2\sqrt{\tilde{E}_P^0}}\int d\tilde{E}_1(\tilde{E}_P^0 - \tilde{E}_1)^2 \cdot N_{\tilde{E}_P^0}n_{\tilde{E}_P^0-\tilde{E}_1}^{ph}\cdot\Theta[(\tilde{E}_P^0-\tilde{E}_1)-\sqrt{\tilde{E}_1}+\sqrt{\tilde{E}_P^0}] \cdot\Theta[-(\tilde{E}_P^0-\tilde{E}_1)+\sqrt{\tilde{E}_1}+\sqrt{\tilde{E}_P^0}]\cdot\Theta(\tilde{E}_1-\tilde{E}_P^0). \tag{A5}$$

Inserting the integration limits instead of using the Heaviside functions results in

$$\frac{\partial}{\partial t}N_{\tilde{E}_P^0} = -\frac{N_{\tilde{E}_P^0}}{2\tau_{sc}\sqrt{\tilde{E}_P^0}}\int_{(\sqrt{\tilde{E}_P^0}-1)^2}^{(\sqrt{\tilde{E}_P^0}+1)^2} d\tilde{E}_1\cdot(\tilde{E}_P^0-\tilde{E}_1)^2 n_{\tilde{E}_1-\tilde{E}_P^0}^{ph}, \tag{A6}$$

which is identical to Eq. (5).

2. Transmission of inhomogeneous sample

In the following we derive the transmission of a sample consisting of layers with slightly different resonances. As we do not take into account reflection at the back surface, in the sample two polaritons modes E_1 and E_2 propagate in the sample. The Maxwell conditions at the boundary between two layers with indices $j-1$ and j and thicknesses d_{j-1} and d_j are

$$\begin{aligned} E_1^{j-1}\exp(ik_1^{j-1}d_{j-1}) + E_2^{j-1}\exp(ik_2^{j-1}d_{j-1}) &= E_1^j + E_2^j, \\ n_1^{j-1}E_1^{j-1}\exp(ik_1^{j-1}d_{j-1}) + n_2^{j-1}E_2^{j-1}\exp(ik_2^{j-1}d_{j-1}) &= n_1^jE_1^j + n_2^jE_2^j. \end{aligned} \tag{A7}$$

Solving the equation for E_1^j and E_2^j results in

$$\begin{aligned} E_1^j(\omega) = \frac{1}{k_1^j(\omega)-k_2^j(\omega)}\cdot\{&[k_1^{j-1}(\omega) - k_2^j(\omega)]E_1^{j-1}(\omega)\exp[ik_1^{j-1}(\omega)d_{j-1}] + [k_2^{j-1}(\omega) - k_2^j(\omega)]E_2^{j-1}(\omega)\exp[ik_2^{j-1}(\omega)d_{j-1}]\}, \\ E_2^j(\omega) = \frac{1}{k_2^j(\omega)-k_1^j(\omega)}\cdot\{&[k_1^{j-1}(\omega) - k_1^j(\omega)]E_1^{j-1}(\omega)\exp[ik_1^{j-1}(\omega)d_{j-1}] + [k_2^{j-1}(\omega) - k_1^j(\omega)]E_2^{j-1}(\omega)\exp[ik_2^{j-1}(\omega)d_{j-1}]\}. \end{aligned} \tag{A8}$$

If we additionally assume Pekar's ABC at the front surface as discussed in Sec. II, the electric field transmitted through a sample with n layers can then be calculated by the set of equations,

$$E(d,\omega) = E_1^n(\omega)\cdot\exp[ik_1^n(\omega)d_n] + E_2^n(\omega)\cdot\exp[ik_2^n(\omega)d_n],$$

$$E_1^j(\omega) = \begin{cases} a_1(\omega) & j=1 \\ \frac{1}{k_1^j(\omega)-k_2^j(\omega)}\{[k_1^{j-1}(\omega)-k_2^j(\omega)]E_1^{j-1}(\omega)\exp[ik_1^{j-1}(\omega)d_{j-1}] + [k_2^{j-1}(\omega)-k_2^j(\omega)]E_2^{j-1}(\omega)\exp[ik_2^{j-1}(\omega)d_{j-1}]\} & j\neq 1, \end{cases} \tag{A9}$$

$$E_2^j(\omega) = \begin{cases} a_2(\omega) & j=1 \\ \frac{1}{k_2^j(\omega)-k_1^j(\omega)}\{[k_1^{j-1}(\omega)-k_1^j(\omega)]E_1^{j-1}(\omega)\exp[ik_1^{j-1}(\omega)d_{j-1}] + [k_2^{j-1}(\omega)-k_1^j(\omega)]E_2^{j-1}(\omega)\exp[ik_2^{j-1}(\omega)d_{j-1}]\} & j\neq 1. \end{cases}$$

This recursive representation of the equations is basically the product of the electric field transmitted through each layer.

*jan.brandt@tu-dortmund.de

[1] M. H. Anderson, J. R. Ensher, M. R. Matthews, C. E. Wieman, and E. A. Cornell, Science **269**, 198 (1995).
[2] K. B. Davis, M. O. Mewes, M. R. Andrews, N. J. van Druten, D. S. Durfee, D. M. Kurn, and W. Ketterle, Phys. Rev. Lett. **75**, 3969 (1995).
[3] D. Snoke, Science **298**, 1368 (2002).
[4] G. Baldassarri Höger von Högersthal, G. Dasbach, D. Fröhlich, M. Kulka, H. Stolz, and M. Bayer, J. Lumin. **112**, 25 (2005).
[5] J. Brandt, D. Fröhlich, C. Sandfort, M. Bayer, H. Stolz, and N. Naka, Phys. Rev. Lett. **99**, 217403 (2007).
[6] N. Naka and N. Nagasawa, Phys. Rev. B **65**, 075209 (2002).
[7] D. Fishman, C. Faugeras, M. Potemski, A. Revcolevschi, and P. H. M. van Loosdrecht, Phys. Rev. B **80**, 045208 (2009).
[8] C. Sandfort, J. Brandt, D. Fröhlich, M. Bayer, and H. Stolz, Phys. Rev. B **78**, 045201 (2008).
[9] J. I. Jang and J. P. Wolfe, Phys. Rev. B **74**, 045211 (2006).
[10] A. L. Ivanov, C. Ell, and H. Haug, Phys. Rev. E **55**, 6363 (1997); C. Ell, A. L. Ivanov, and H. Haug, Phys. Rev. B **57**, 9663 (1998).
[11] K. E. O'Hara, Ph.D. thesis, University of Illinois, 1999.
[12] T. Tayagaki, A. Mysyrowicz, and M. Kuwata-Gonokami, J. Phys. Soc. Jpn. **74**, 1423 (2005).
[13] D. Fröhlich, A. Kulik, B. Uebbing, A. Mysyrowicz, V. Langer, H. Stolz, and W. von der Osten, Phys. Rev. Lett. **67**, 2343 (1991); D. Fröhlich, A. Kulik, B. Uebbing, V. Langer, H. Stolz, and W. von der Osten, Phys. Status Solidi B **173**, 31 (1992).
[14] J. Brandt, D. Fröhlich, C. Sandfort, M. Bayer, and H. Stolz, Phys. Status Solidi C **6**, 556 (2009).
[15] G. Baldassarri Höger von Högersthal, D. Fröhlich, M. Kulka, Th. Auer, M. Bayer, and H. Stolz, Phys. Rev. B **73**, 035202 (2006).
[16] S. I. Pekar, Sov. Phys. JETP **6**, 785 (1958).
[17] A. Puri and J. L. Birman, Phys. Rev. A **27**, 1044 (1983).
[18] Y. Petroff, P. Y. Yu, and Y. R. Shen, Phys. Rev. B **12**, 2488 (1975).
[19] H.-R. Trebin, H. Z. Cummins, and J. L. Birman, Phys. Rev. B **23**, 597 (1981).
[20] G. White, J. Phys. C **11**, 2171 (1978).
[21] D. Fröhlich, J. Brandt, C. Sandfort, M. Bayer, and H. Stolz, Phys. Status Solidi B **243**, 2367 (2006).
[22] G. Pollack, Rev. Mod. Phys. **41**, 48 (1969).